2014 5th IEEE RAS & EMBS International Conference on
Biomedical Robotics and Biomechatronics (BioRob)
August 12-15, 2014. São Paulo, Brazil

Dipole Field Navigation for Targeted Drug Delivery

Maxime Latulippe, *Student Member*, *IEEE*, and Sylvain Martel, *Senior Member*, *IEEE*

***Abstract*— A new method for the navigation of therapeutic agents in the vascular network is introduced. This method, dubbed Dipole Field Navigation (DFN), is characterized by high directional gradients and a high magnetic field strength. The latter is used to bring magnetic therapeutic agents at saturation magnetization such that when combined with high directional gradients, effective navigation at any depths within the patient can be achieved. DFN does not have many of the constraints of gradient coil-based platforms, which include potential peripheral nerve stimulations, reduced directional changes and slew rates of the gradient fields, overheating of the coils, and high implementation cost. To achieve such specifications, soft ferromagnetic cores are positioned at specific locations inside the tunnel of a clinical MRI scanner providing a high uniform field of typically up to 3 T, sufficient to bring both the cores and the therapeutic agents at full saturation magnetization. The field distortions created by the cores result in gradients exceeding 300 mT/m for whole body interventions. Hence, with such cores placed at specific locations, the resulting gradients would cause the therapeutic agents to follow a precise path in the vascular network towards the targeted region. In this paper, the fundamental theory of DFN with preliminary *in vitro* experimental results using one core in a 1.5 T scanner confirms the potential of DFN for targeted drug delivery.**

I. INTRODUCTION

Although most cancers are localized, therapeutic agents are still injected systematically in the vascular network. This approach leads to a suboptimal amount of therapeutics in the region to be treated while affecting healthy organs and tissues. As such, the concept of Direct Targeting (DT) [1] has been introduced, where the therapeutic agents are navigated in the vascular network directly from the injection site towards the region to be treated. Typically, such navigable therapeutic agents consist of magnetic nanoparticles (MNP) being embedded with therapeutics in a spherical matrix. The MNP, which are typically superparamagnetic nanoparticles, provide means for inducing directional pulling forces on the agents, while acting as MRI contrast agents for tracking or targeting efficacy assessment. The superparamagnetic nanoparticles see their magnetization increase up to a saturation magnetization value when submitted to an increasing magnetic field strength, and lose their magnetization when they are not exposed to a magnetic field. Such a magnetic property allows the use of magnetic gradients to induce directional pulling forces for navigation purposes, while avoiding aggregations of the therapeutic agents once the patient is removed from the interventional platform. Hence, for a given effective volume of superparamagnetic nanoparticles being embedded in each navigable therapeutic agent, both the magnetic field strength and the magnetic gradients must be maximized to achieve more effective navigation and better targeting in deep tissues.

Fast directional changes of the magnetic gradients are typically required for endovascular navigation of therapeutic agents. Known magnetic navigation platforms having this capability can be categorized as Electromagnetic Actuation Magnetic Navigation Systems (EMA-MNS) and Magnetic Resonance Navigation (MRN) platforms [1]. The rapid decay of the magnetic field strength of EMA-MNS leads to suboptimal directional pulling forces being induced on the agents when operating in deeper regions of the body. As such, MRN has been proposed where directional imaging gradients are superposed on the high uniform field of a clinical MRI scanner [2], [3]. While the magnetic field strength inside the tunnel of the scanner can be sufficient to achieve depth independent saturation magnetization of the nanoparticles, MRN lacks the maximum gradient magnitude achievable with EMA-MNS. Additional coil inserts can provide much higher gradients [4], but the smaller inner diameter of the insert prevents whole body interventions to be conducted. Although whole body MRN could be done using ultra-high gradient scanners, these platforms are much more expensive, not widely available, and the operating time for MRN conducted in complex networks is limited due to excessive heating of the coils caused by switching gradients.

To overcome these limitations, a new method dubbed Dipole Field Navigation (DFN) is introduced. Magnetic gradients in DFN are created by the distorted high uniform magnetic field of a clinical MRI system when one or several ferromagnetic cores are placed inside the tunnel of the scanner. When positioned adequately, such cores create a pattern of magnetic gradients that entail the therapeutic agents (at saturation magnetization) to follow a precise path in the vascular networks. In this paper, a first insight of some theoretical aspects of DFN is presented, along with preliminary experimental results.

II. THEORY

The magnetic field $\mathbf{B}_0$ inside an MRI tunnel can be considered static and uniform. A soft ferromagnetic core placed in such a field induces a magnetic field $\mathbf{B}_{core}$ that adds to $\mathbf{B}_0$, distorting the total resultant field in the tunnel:

$$\mathbf{B} = \mathbf{B}_0 + \mathbf{B}_{core} \tag{1}$$

This work was funded by the Fonds Québécois de la Recherche sur la Nature et les Technologies (FQRNT) and by the Research Chair of École Polytechnique (CREP) in nanorobotics. The MRI scanner used was acquired with the financial support of the Canada Foundation for Innovation (CFI).

Maxime Latulippe is with the NanoRobotics Laboratory, Dept. of Comp. and Soft. Eng., Institute of Biomedical Eng., Polytechnique Montréal, QC, Canada (maxime.latulippe@polymtl.ca).

Sylvain Martel (corresponding author) is the Director of the NanoRobotics Laboratory, Dept. of Comp. and Soft. Eng., Institute of Biomedical Eng., Polytechnique Montréal, QC, Canada (sylvain.martel@polymtl.ca).

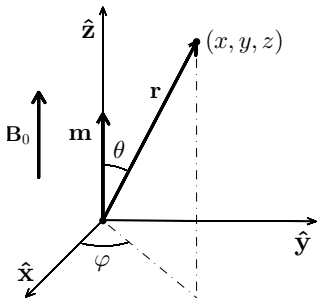

Fig. 1. Convention used.

For a uniformly magnetized spherical bead of radius R, the induced magnetic field at any point $\mathbf{r} = (x, y, z)$ around the bead is that of a dipole of equal magnetic moment $\mathbf{m}$ placed at the center of the bead:

$$\mathbf{B}_{dip}(r > R) = \frac{\mu_0}{4\pi}\left[3\frac{(\mathbf{m}\cdot\mathbf{r})\mathbf{r}}{r^5} - \frac{\mathbf{m}}{r^3}\right] \quad [T] \tag{2}$$

where $\mu_0 = 4\pi \times 10^{-7} H/m$ is the vacuum permeability and $r = |\mathbf{r}|$. In the following, let $\mathbf{B}_0 = B_0\hat{\mathbf{z}}$ be aligned with the z-axis. For a sphere, the magnetic moment is then given by

$$\mathbf{m} = \frac{4\pi R^3}{3} M\hat{\mathbf{z}} \qquad [A \cdot m^2] \tag{3}$$

where M is the volume magnetization of the ferromagnetic material, which depends on the static field density B_0. The vector $\mathbf{m}$ being parallel to $\hat{\mathbf{z}}$, Eq. (2) becomes

$$\mathbf{B}_{dip} = \frac{\mu_0 m}{4\pi r^5}\left[3xz\hat{\mathbf{x}} + 3yz\hat{\mathbf{y}} + (3z^2 - r^2)\hat{\mathbf{z}}\right] \tag{4}$$

which highlights the symmetry of $\mathbf{B}$ around $\hat{\mathbf{z}}$ in our case.

The force and torque exerted on a particle of magnetic moment $\mathbf{m}_p$ placed in a magnetic field $\mathbf{B}$ are given by

$$\mathbf{F}_{mag} = (\mathbf{m}_p \cdot \nabla)B = \nabla(\mathbf{m}_p \cdot \mathbf{B}) \tag{5}$$

$$\boldsymbol{\tau}_{mag} = \mathbf{m}_p \times \mathbf{B} \tag{6}$$

In our case, particles (therapeutic agents) are magnetized by the total field $\mathbf{B}$, which implies that $\mathbf{m}_p$ is aligned with $\mathbf{B}$. Therefore, the latter equations simplify to

$$\mathbf{F}_{mag} = \nabla(m_p B) = m_p \nabla B \tag{7}$$

$$\boldsymbol{\tau}_{mag} = 0 \tag{8}$$

Note that the magnetization of the particle in fact contributes to the total field $\mathbf{B}$, but since its radius $R_p \ll R_{core}$ is very small, we neglect this contribution as well as its effect on the magnetization of the core.

To further simplify Eq. (7), we consider the case where the particles are located *far enough* from the core so that the influence of $\mathbf{B}_{core}$ on $\mathbf{m}_p$ is negligible (*far enough* is defined below). Following this condition, $\mathbf{m}_p$ is approximately parallel to $\hat{\mathbf{z}}$, hence

$$\mathbf{F}_{mag} \approx m_p \nabla B_z \tag{9}$$

thus the magnetic force induced on a particle is aligned with the gradient of the z-component of $\mathbf{B}$ at the particle location.

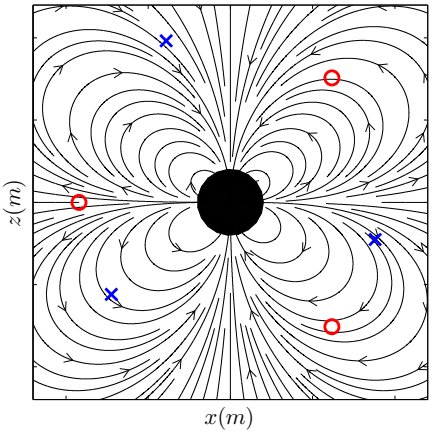

Fig. 2. Magnetic gradient field around a magnetized spherical core. Blue crosses and red circles show different locations around the core where the orientation of the gradient is $\frac{3\pi}{4}$ and $-\frac{\pi}{2}$ respectively. Note that the field line density is not proportional to the gradient magnitude.

For a spherical magnetic core, calculating the derivative of B_z yields (using Eq. (4))

$$\mathbf{G} \equiv \nabla B_z = \nabla\left(B_0 + \frac{\mu_0 m}{4\pi}\frac{3z^2 - r^2}{r^5}\right) \tag{10}$$

$$= \frac{3\mu_0 m}{4\pi r^7}\begin{bmatrix} x\left(r^2 - 5z^2\right) \\ y\left(r^2 - 5z^2\right) \\ z\left(3r^2 - 5z^2\right) \end{bmatrix}^T \tag{11}$$

Using the convention illustrated at Fig.1, we substitute $x = r\sin\theta\cos\varphi$, $y = r\sin\theta\sin\varphi$ and $z = r\cos\theta$ to get

$$\mathbf{G} = \frac{3\mu_0 m}{4\pi r^4}\begin{bmatrix} \sin\theta\cos\varphi\left(1 - 5\cos^2\theta\right) \\ \sin\theta\sin\varphi\left(1 - 5\cos^2\theta\right) \\ \cos\theta\left(3 - 5\cos^2\theta\right) \end{bmatrix}^T \tag{12}$$

We take advantage of the symmetry of $\mathbf{G}$ around $\hat{\mathbf{z}}$ and express the gradient in 2D in the xz-plane. Posing $\varphi = 0$, the gradient simplifies to

$$\mathbf{G} = \frac{3\mu_0 m}{4\pi r^4}\begin{bmatrix} \sin\theta\left(1 - 5\cos^2\theta\right) \\ \cos\theta\left(3 - 5\cos^2\theta\right) \end{bmatrix}^T \tag{13}$$

Fig. 2 shows the gradient field around a magnetized spherical core and depicts locations where the same gradient is obtained, for two arbitrarily chosen gradients.

Substituting $\nabla B_z = \mathbf{G}$ in Eq. (9) finally gives an expression for the induced magnetic force between two dipoles with parallel magnetizations (i.e. a core and a particle) as a function of r, the distance of the particle to the center of the core, and θ, the angle between $\mathbf{r}$ and $\hat{\mathbf{z}}$. Note that this result is equivalent to the one obtained by Fujita and Mamiya [5]. The force is purely attractive when $\theta = 0$ or $\theta = \pi$ and purely repulsive when $\theta = \pi/2$ or $\theta = -\pi/2$.

The variation of the force magnitude between two dipoles as the inverse fourth power of r was validated experimentally in the far field [6]–[8]. In particular, Mehdizadeh *et al.* [8] has shown this relation to be accurate when $r/R > 4$ (for two identical soft ferromagnetic spheres). At smaller distances, the magnetization of one sphere affects the magnetization

of the other and vice-versa, leading to an underestimated attractive force when $\theta \in \{0, \pi\}$ (increased magnetizations) and an overestimated repulsive force when $\theta \in \{-\pi, \pi\}$ (decreased magnetizations). Mehdizadeh *et al.* [8] show that the change in the magnetization can be described using a simple dipole model, and thereby precisely correcting the magnetization values allows to use the same inverse 4th power law when $r/R < 4$. Their model, however, applies only when the magnetization of the spheres lies in the linear region of the magnetization curve, which is not our case. In fact, one of the advantages of working inside the tunnel of an MRI is that the core and the particles reach the saturation magnetization, thus maximizing the pulling force induced on particles. The variation of the magnetization as a function of the magnetic field density B being much lower when at saturation, it is reasonable to suppose that the dipole-dipole interaction effect is negligible from a closer distance $\mathbf{r}$ in our case. Moreover, because $R_p \ll R_{core}$, it is likely that the interaction effect between the core and particles is weaker than for two identical beads. For these reasons, we consider $r/R_{core} > 4$ to be a worst case limit for the validity of the above results in our case. Here, we conservatively use this constraint to define *far enough*, introduced to obtain Eq. (9).

III. METHOD

We propose to place soft ferromagnetic cores inside an MRI tunnel to distort the field $\mathbf{B}_0$ so that the resultant magnetic gradient field makes injected particles follow a predefined path inside the vascular network. More precisely, the particles, transported by the blood flow, must bifurcate in the appropriate vessel branches towards a target region.

This navigation problem consists in correctly positioning cores such that appropriate magnetic gradients are generated at different locations inside the patient's body. In particular, gradients are needed before each vessel intersection to push the particles inside the desired branch.

In this paper, we address the simplified problem of positioning a single spherical core only.

A. Core positioning

Starting from the expression for the magnetic gradient field around a dipole as a function of $\mathbf{r}$ (Eq. (12) and Eq. (13)), we are interested in solving the inverse problem. In other words, we want to position a core such that the resultant magnetic gradient $\mathbf{G} = (G, \theta_G, \varphi_G)$ at a target point $\mathbf{p}$ has a given magnitude and orientation. Similar problems have been solved to localize dipoles when the magnetic field and its gradient tensor are known at a certain point [9], [10]. In our case, where only the gradient at $\mathbf{p}$ is known, the localization problem is ill-posed: for any given gradient, there are always three solutions (see Fig. 2). Here, we develop a simple approach to calculate these three positions.

The symmetry of the magnetic gradient field around $\hat{\mathbf{z}}$ allows to first solve the inverse problem in 2D. We define the plane Π, centered at $\mathbf{p}$ and oriented such that the vectors $\mathbf{m}$ and $\mathbf{G}$ lie on this plane. Recall that $\mathbf{m}$ is parallel to $\hat{\mathbf{z}}$, thus the orientation of Π can be defined, relative to the xz-plane, by a rotation around $\hat{\mathbf{z}}$ by the angle φ_G . Consequently, the 2D positioning solution will apply on plane Π. From Eq. (13),

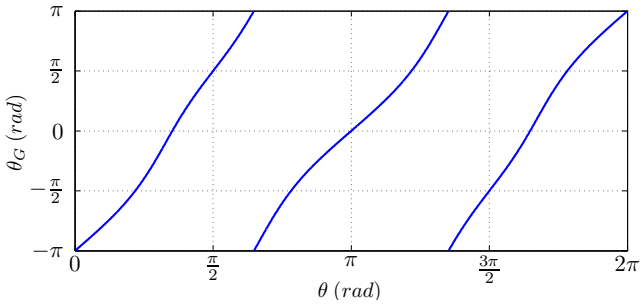

Fig. 3. Magnetic gradient angle θ_G as a function of the angle θ.

$$\tan\theta_G = \frac{\sin\theta\left(1 - 5\cos^2\theta\right)}{\cos\theta\left(3 - 5\cos^2\theta\right)} = \frac{a}{b} \tag{14}$$

$$G = \frac{3\mu_0 m}{4\pi r^4}\sqrt{a^2 + b^2} \tag{15}$$

where the substitution variables a and b are introduced to simplify the latter equation. The relation at Eq. (14) between θ_G and θ is plotted at Fig. 3. We see that for any orientation of the desired magnetic gradient at $\mathbf{p}$, there are three solutions for θ. Although θ cannot be isolated in this equation, these solutions can be found numerically by, for example, interpolating precomputed values in a lookup table. Then, calculating the distance r for each value of θ is straightforward using Eq. (15), resulting in three possible positions of the target point $\mathbf{p}$ relative to the core position. Or, equivalently, the three possible core positions, $\mathbf{d}_1^\Pi$, $\mathbf{d}_2^\Pi$ and $\mathbf{d}_3^\Pi$, relative to $\mathbf{p}$ and expressed in Π, are given by

$$\mathbf{d}_i^\Pi = \begin{bmatrix} -r_i \sin\theta_i \\ -r_i \cos\theta_i \end{bmatrix} = \begin{bmatrix} d_{i,x}^\Pi \\ d_{i,z}^\Pi \end{bmatrix} \quad i = 1, 2, 3 \tag{16}$$

in Cartesian coordinates. We emphasize that in 3D, for any angle φ_G, the three possible core positions lie on the plane Π. The extension to the 3D solution in the xyz global frame therefore involves a rotation of the 2D positions $\mathbf{d}_i^\Pi$ by an angle φ_G around $\hat{\mathbf{z}}$ and a translation by $\mathbf{p}$:

$$\mathbf{d}_i = R_z(\varphi_G)\mathbf{d}_i^\Pi + \mathbf{p} \tag{17}$$

$$= \begin{bmatrix} \cos\varphi_G & -\sin\varphi_G & 0 \\ \sin\varphi_G & \cos\varphi_G & 0 \\ 0 & 0 & 1 \end{bmatrix} \begin{bmatrix} d_{i,x}^\Pi \\ 0 \\ d_{i,z}^\Pi \end{bmatrix} + \mathbf{p} \tag{18}$$

$$= \begin{bmatrix} d_{i,x}^\Pi \cos\varphi_G \\ d_{i,x}^\Pi \sin\varphi_G \\ d_{i,z}^\Pi \end{bmatrix} + \mathbf{p} \qquad i = 1, 2, 3 \tag{19}$$

B. Positioning regions

The solution detailed above for the magnetic gradient inverse problem allows to find the optimal positions of a core in order to induce a specific gradient at a target point $\mathbf{p}$. In practice however, placing the core at one of these positions might not be possible due to physical constraints.

A more practical solution is therefore to define constraints on the desired gradient, in particular a maximum orientation

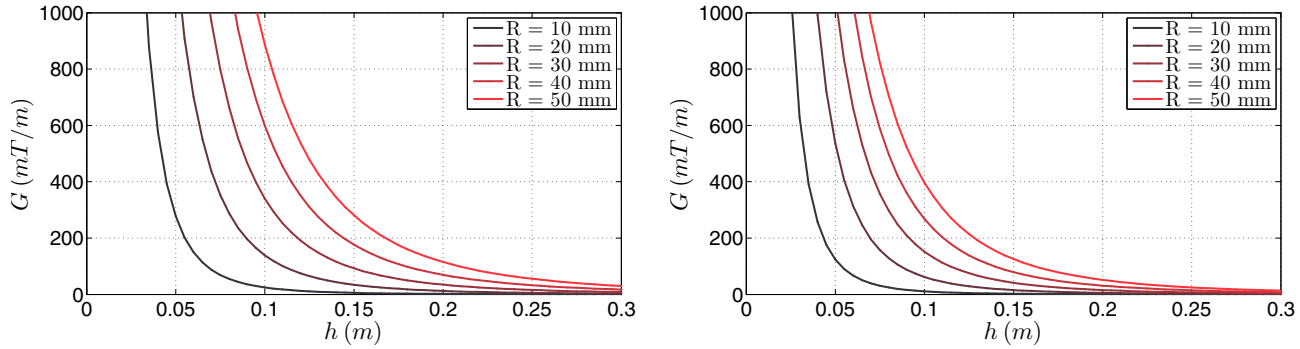

(a) $\theta = 0$ (b) $\theta = 0.352\pi$

Fig. 4. Maximum ($\theta = 0$) and minimum ($\theta = 0.352\pi$) gradients as a function of h, for different spherical core radii (carbon steel, $M = 1.43{\times}10^6$A/m).

error angle ξ_{max} from the desired orientation (θ_G, φ_G) and a minimum magnitude G_{min}. These parameters should be defined by taking into account hemodynamic properties, such as blood viscosity and flow velocity, bifurcation angles and radii of curvature, as well as the magnetic specifications of the injected particles. We do not address this question here and let it for future investigations. The sets of core positions (positioning regions) respecting the constraints on the desired gradient can be defined by closed volumes (surfaces in 2D).

C. Core size

It was previously shown that magnetic gradients in the order of at least 200-400 mT/m are desirable in order to control ferromagnetic therapeutic agents inside blood vessels [4], [11]. Because the gradient magnitude around a dipole decreases at a fast rate of $1/r^4$, it is of interest to investigate how far from a core such gradient magnitudes can be obtained.

More relevant for the following, we define h, the distance of a particle from the core surface:

$$h = r - R_{core} \tag{20}$$

The gradient magnitude varies, for a fixed distance, as a function of θ. Using Eq. (15), one can find that the maximum gradient $G = 2\frac{3\mu_0 m}{4\pi r^4}$ is obtained at $\theta = 0$ and $\theta = \pi$, whereas the minimum gradient $G \approx 0.9\frac{3\mu_0 m}{4\pi r^4}$ occurs at $\theta \approx \pm 0.352\pi$ and $\theta \approx \pm 0.648\pi$. The gradient magnitude is also function of the core magnetic moment, which depends on the total volume of the core and the material used (see Eq. (3)). For our purpose, a soft ferromagnetic material having a volume magnetization M as high as possible should be used. Given that material, the gradient magnitude at a distance h is function of the core size.

Fig. 4 plots the theoretical maximum and minimum gradient magnitudes, calculated at $\theta = 0$ and $\theta = 0.352\pi$ respectively (using Eq. (15)), as a function of h for different spherical core radii. These curves correspond to our carbon steel balls magnetized at 1.5 T, for which the volume magnetization is $M_{1.5T} = 1.43{\times}10^6$A/m. At 10 cm from the core surface, which distance would allow to reach most regions inside a patient's body, we see that a core of radius $R = 3$ cm is sufficient to produce a gradient of more than 300 mT/m in the best case ($\theta = 0$). To ensure a minimum gradient of the same magnitude in the worst case ($\theta \approx 0.352\pi$) however, a core of radius between 4 cm and 5 cm is needed.

IV. EXPERIMENTS

The feasibility of endovascular navigation using the proposed method was tested *in vitro* by attempting to control the direction of magnetic particles at a junction.

Our setup consisted in a T-shaped glass tube having a constant circular cross-section of 3 mm in diameter and splitting in two branches: one going straight and one bifurcating at 90°. The input of the tube was connected to a syringe pump (Harvard Apparatus PHD 2000) delivering a constant flow of 60 ml/min, which is representative of some arteries in the human body. This yielded an average flow velocity of 14 cm/s before the junction. We did not consider the pulsatile nature of the blood flow to keep the setup simple. A solution of 36% (vol.) glycerol in water was used as a blood analogue fluid [12], which has a dynamic viscosity of 3.5 mPa·s.

The T-shaped tube was fixed on a LEGO® baseplate and centered in the tunnel of a Siemens Avanto MRI scanner having a static field density $B_0 = 1.5$ T. It was oriented such that it was parallel to the horizontal xz-plane, with the two bifurcations angled at 45° from $\hat{\mathbf{z}}$. A carbon steel spherical core of radius $R_{core} = 12.7$ mm, having a volume magnetization $M_{1.5T} = 1.43{\times}10^6$A/m at 1.5 T, was glued onto a pile of LEGO blocks, which provided the ability to quickly and precisely change the core position on the baseplate during the experiments. We ensured that the core center was vertically aligned with the center of the T-shaped tube (along the y-axis). The core could then be positioned according to the baseplate grid, defined by a stud spacing of 8 mm. We considered the core saturated, as its magnetization at 1.0 T, $M_{1.0T} = 1.41{\times}10^6$A/m, is 1.3% less than $M_{1.5T}$.

In order to test the proposed method, we attempted to guide magnetic particles inside each of the bifurcations separately. The arrangement of the setup allowed solving the core positioning problem in 2D for simplicity. The target point was set 5 mm upstream of the junction center. The desired gradient orientations were defined as $\theta_G = -\pi/4$ and $\theta_G = 3\pi/4$ for the left and right bifurcation respectively. Note that these gradients are orthogonal to the flow in order to push the particles on the desired side of the tube, past the centerline, as

detailed in [4]. We defined $G_{min} = 300\,\text{mT/m}$, $\xi_{max} = \pi/8$ and respected the constraint $r/R_{core} > 4$. Fig. 5 depicts the setup and shows the core positioning regions (surfaces) corresponding to each bifurcation. The surface vertices were obtained by calculating the core positions corresponding to the constraint limits. The matching core positions on the baseplate are marked by small gray crosses. Four of these positions were tested (two per bifurcation), which are identified by larger black crosses. To reference them later, the tested positions are identified $\mathbf{d}_{L,1}$, $\mathbf{d}_{L,2}$ and $\mathbf{d}_{R,1}$, $\mathbf{d}_{R,2}$, for sending particles in the left and right bifurcations respectively (see Fig. 5). The two remaining positioning regions could not be tested due to the core colliding with the tubing at these positions.

For each of the tested positions, ferrofluid was injected upstream of the T-shaped tube in order to generate magnetic particles in the flow. The ferrofluid used (Ferrotec EFH1) has a volume magnetization $M_{1.0T} = 17\,240\,\text{A/m}$ at $1.0\,\text{T}$ and $M_{1.5T} = 17\,580\,\text{A/m}$ at $1.5\,\text{T}$ (2% increase). Thus, it was considered to be saturated at $1.5\,\text{T}$. When injected, the ferrofluid formed small aggregations in the direction of $\mathbf{B}_0$. A MRI-compatible camera (MRC Systems GmbH model 12M) was placed above the junction and recorded the motion of the ferrofluid aggregations during the injection (640×480 pixels, 30 frames per second). The average video duration over the four tested positions was $19\,\text{s}$. A differential analysis was performed on each video in order to detect moving aggregates from frame to frame. A density plot of the detected motion was then superimposed on the average video frame.

V. RESULTS AND DISCUSSION

Fig. 6 shows the navigation results obtained by positioning the core at $\mathbf{d}_{L,1}$, $\mathbf{d}_{L,2}$, $\mathbf{d}_{R,1}$ and $\mathbf{d}_{R,2}$ (each row corresponding to one position, in order). The first column depicts the calculated gradient field around the junction and the theoretical resulting gradient at $\mathbf{p}$. The second and third columns show raw images from the videos and images resulting from the motion detection process, respectively. On the latter, red color depicts areas of highest motion density, whereas blue depicts those of lowest density.

In each of these tests, the navigation attempt was successful as the results show the ferrofluid aggregates bifurcating in the desired branch. In particular, motion was detected only in the desired branch for positions $\mathbf{d}_{L,2}$, $\mathbf{d}_{R,1}$ and $\mathbf{d}_{R,2}$. At position $\mathbf{d}_{L,1}$, we see a region of low motion density in the wrong branch. In the corresponding video, we observed tiny boluses ($\approx$10-20 times smaller than the other aggregates) bifurcating in the wrong branch. In fact, such tiny boluses were also observed in the wrong branch for $\mathbf{d}_{L,1}$, but they were not significant enough to appear on the motion density plot in that case. As for the other positions, a single tiny bolus was seen taking the wrong branch for $\mathbf{d}_{R,1}$ and none for $\mathbf{d}_{R,2}$.

Although the targeting efficiency was not quantified, we can affirm based on these results that the vast majority of the ferrofluid aggregates was guided successfully in the desired bifurcation. This clearly demonstrates that it is possible to control the direction of magnetic particles at a vessel junction using the proposed method.

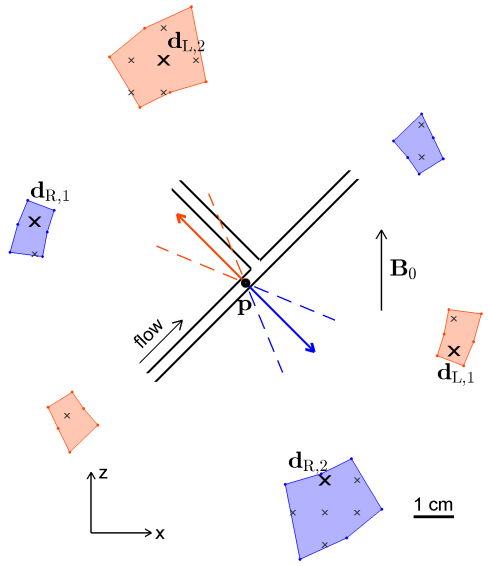

Fig. 5. Illustration of the experimental setup. The blue and orange arrows depict the desired gradient orientations, while dashed lines depict the gradient orientations corresponding to ξ_{max}. The blue and orange surfaces depict the core positioning regions for the corresponding gradient color. Positions on the LEGO baseplate matching theses surfaces are marked by crosses. The tested positions are identified by larger crosses.

VI. CONCLUSION

By adequately positioning ferromagnetic cores inside the tunnel of a MRI system, the magnetic gradients generated by the distorted uniform field entail the therapeutic agents to follow a precise path in the vascular network, towards a targeted region to be treated. This fundamental principle of the new endovascular navigation method introduced in this paper, dubbed Dipole Field Navigation, was demonstrated experimentally using one core in a $1.5\,\text{T}$ MRI scanner. For more complex paths with multiple bifurcations, several cores would be needed and positioned by considering, and possibly exploiting, the magnetic dipole-dipole interaction.

The high field strength inside the tunnel of the scanner is sufficient to bring the magnetization of both the cores and the navigable therapeutic agents close or at full saturation magnetization. As such, DFN can provide high directional gradients comparable to the ones generated by expensive and complex electromagnetic coil assemblies, while the responsiveness of the therapeutic agents to the applied gradients is maximized. A great advantage of DFN compared to other MRN methods is the potential low price of implementation when used with a MRI scanner since it does not typically require sophisticated and costly hardware.

Another advantage is the non-requirement for switching (dynamically changing) gradients, that are limited in their slew (transition) rate due to technological and/or physiological constraints (e.g. safety issues such as peripheral nerve stimulation for the patient) and other limiting factors such as an overheating of the coils. But such advantages are paid by the requirement to develop sophisticated models to predict the effect of the cores on the navigable agents, which may become complex especially when dipole-dipole interaction

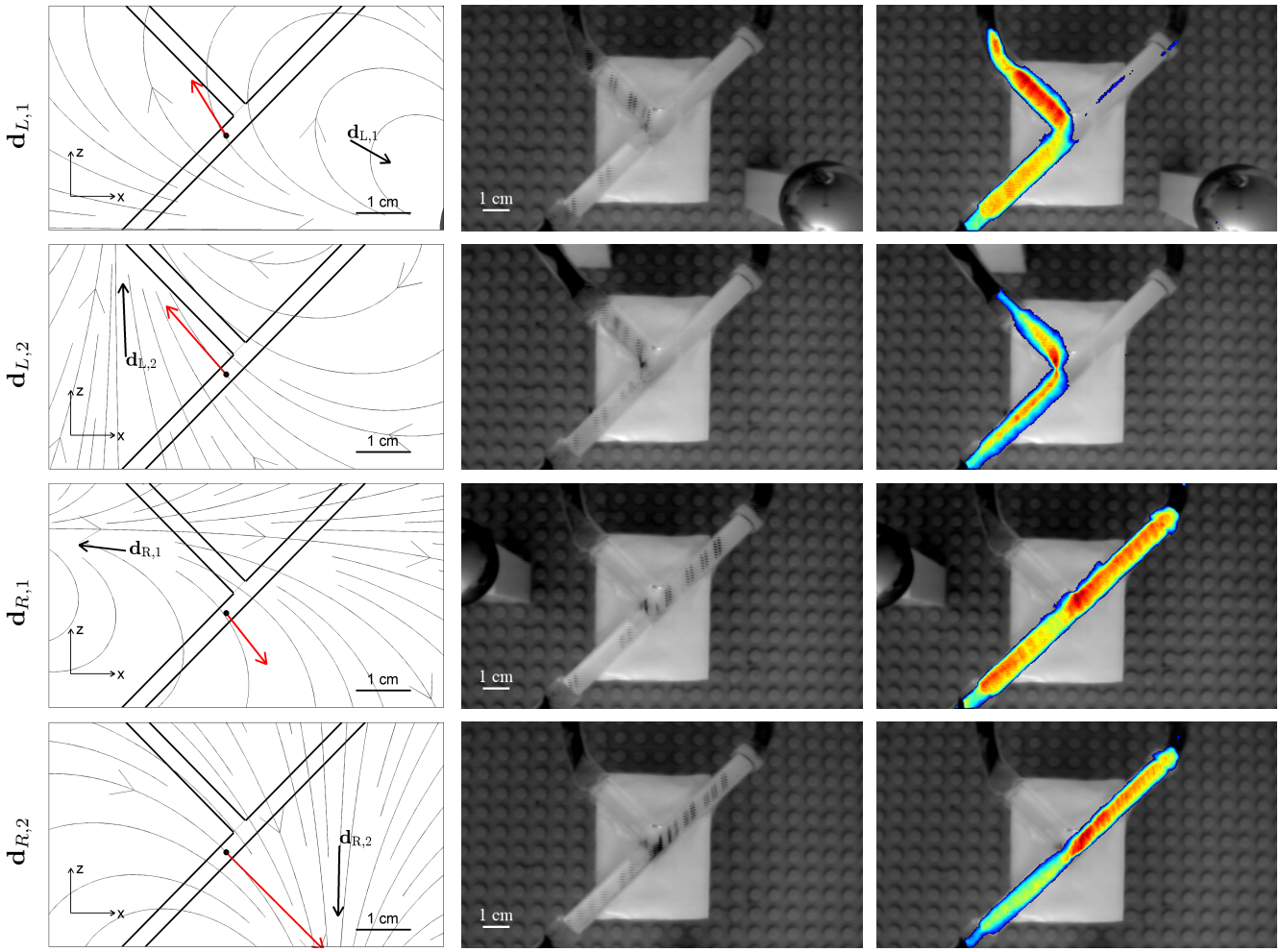

Fig. 6. Navigation results for the tested core positions. Each row corresponds, from top to bottom, to positions $\mathbf{d}_{L,1}$, $\mathbf{d}_{L,2}$, $\mathbf{d}_{R,1}$ and $\mathbf{d}_{R,2}$. The first column depicts the gradient field (gray lines and arrows) around the junction and the gradient at the target point (red arrow, length proportional to the gradient magnitude using the conversion factor 1 T/m $\equiv$ 3 cm). The position of the core is indicated by a thick black arrow. The second column shows raw images from the videos, without any processing. The third column shows composite images obtained by superimposing the motion density plot on the average video frames (red is the highest motion density, blue is the lowest). This figure is best viewed in colors (see the online version).

occurs. Another drawback is the difficulty of tracking the navigable agents in real-time in order to apply corrective actions accordingly during their transit towards the targeted region. This latter issue emphasizes the need for accurate models and the requirement to assess the targeting efficacy on a need basis depending on the expected motion artifacts being encountered during the intervention.

REFERENCES

[1] S. Martel, "Magnetic Therapeutic Delivery Using Navigable Agents," *J. of Therapeutic Delivery*, vol. 5, no. 2, pp. 189–204, 2014.

[2] J.-B. Mathieu, G. Beaudoin, and S. Martel, "Method of Propulsion of a Ferromagnetic Core in the Cardiovascular System through Magnetic Gradients Generated by an MRI System." *IEEE Trans. Biomed. Eng.*, vol. 53, no. 2, pp. 292–299, 2006.

[3] S. Martel, J.-B. Mathieu, O. Felfoul, A. Chanu, E. Aboussouan, S. Tamaz, P. Pouponneau, L. Yahia, G. Beaudoin, G. Soulez, and M. Mankiewicz, "Automatic Navigation of an Untethered Device in the Artery of a Living Animal using a Conventional Clinical Magnetic Resonance Imaging System," *Appl. Phys. Lett.*, vol. 90, no. 11, 2007.

[4] J.-B. Mathieu and S. Martel, "Steering of Aggregating Magnetic Microparticles using Propulsion Gradients Coils in an MRI Scanner." *Magn. Reson. Med.*, vol. 63, no. 5, pp. 1336–45, 2010.

[5] T. Fujita and M. Mamiya, "Interaction Forces Between Nonmagnetic Particles in the Magnetized Magnetic Fluid," *J. Magn. Magn. Mater.*, vol. 65, no. 2-3, pp. 207–210, 1987.

[6] R. Castañer, J. M. Medina, and M. J. Cuesta-Bolao, "The Magnetic Dipole Interaction as Measured by Spring Dynamometers," *Am. J. Phys.*, vol. 74, no. 6, pp. 510–513, 2006.

[7] L. E. Gayetsky and C. L. Caylor, "Measuring the Forces Between Magnetic Dipoles," *Phys. Teach.*, vol. 45, no. 6, p. 348, 2007.

[8] A. Mehdizadeh, R. Mei, J. F. Klausner, and N. Rahmatian, "Interaction Forces Between Soft Magnetic Particles in Uniform and Non-Uniform Magnetic Fields," *Acta Mech. Sin.*, vol. 26, no. 6, pp. 921–929, 2010.

[9] V. Y. Epp, G. F. Kopytov, and T. G. Mitrofanova, "Inverse Problem for Static Electromagnetic Field in a Dipole Approximation," *ArXiv Phys. e-prints*, vol. 3, no. physics/0404081, 2004.

[10] T. Nara, S. Suzuki, and S. Ando, "A Closed-Form Formula for Magnetic Dipole Localization by Measurement of its Magnetic Field and Spatial Gradients," *IEEE Trans. Magn.*, vol. 42, no. 10, pp. 3291–3293, 2006.

[11] P. Pouponneau, J.-C. Leroux, G. Soulez, L. Gaboury, and S. Martel, "Co-encapsulation of magnetic nanoparticles and doxorubicin into biodegradable microcarriers for deep tissue targeting by vascular MRI navigation." *Biomaterials*, vol. 32, no. 13, pp. 3481–6, 2011.

[12] W. L. Lim, Y. T. Chew, T. C. Chew, and H. T. Low, "Pulsatile Flow Studies of a Porcine Bioprosthetic Aortic Valve in vitro: PIV Measurements and Shear-Induced Blood Damage." *J. Biomech.*, vol. 34, no. 11, pp. 1417–27, 2001.